# Supporting information

# Prediction of Molecular Separation of Polar-Apolar Mixtures on Heterogeneous Metal-Organic Frameworks: HKUST-1

**Tom R.C. Van Assche[a], Tim Duerinck[a], Stijn Van der Perre[a], Gino V. Baron[a], Joeri F.M. Denayer[a]***

[a] Department of Chemical Engineering, Vrije Universiteit Brussel, Pleinlaan 2, 1050 Brussel, Belgium

* Email: joeri.denayer@vub.ac.be.

## 1. Materials and methods

HKUST-1 was obtained from Sigma-Aldrich under the commercial name Basolite C300 and continuously stored in activated state. The *n*-hexane and methanol vapor phase isotherms (313K) were obtained on (I) a gravimetric uptake device (VTI, SGA-100H) using nitrogen as carrier gas as well as (II) a gravimetric uptake device (Hiden Isochema, IGA 002) without carrier gas. Both methods used 7-18 mg samples. The activation procedure for the dynamic uptake method can be found elsewhere (1).

For the breakthrough experiments, HKUST-1 powder was pelletized using methanol. An excess amount of methanol was added to the active material under nitrogen atmosphere, triggering a color change from dark purple to turquoise. The material was subsequently dried under atmospheric conditions. Before pelletization, a few drops of methanol were again added to the dry turquoise powder, and this wet powder was compressed using a press. The methanol additions saturate the free metal sites, also being the initial water adsorption sites (2). This is believed to partially protect the HKUST-1 structure form water attack as water adsorption has been shown to degrade the material. Previously, DMF was also shown to protect HKUST-1 from liquid water damage (3). Additionally the methanol loading of the MOF should help to protect it against compressive damage during pelletization. Methanol saturation prior to pelletization appears an alternative to plastic bag sealing of the press die and powder (4). The resulting MOF cake was broken and sieved, yielding pellets of 0.4-2 mm diameter. Both the powder as pellets were handled to minimize water adsorption from the atmosphere, as the material is susceptible to water damage (1). The experimental isotherms were obtained on HKUST-1 powder, rather than the HKUST-1 compressed pellets used in the breakthrough experiments. Argon porosimetry confirms both the powder as pellets to maintain an almost identical high porosity (figure S.1). The BET surface of the powder was 1885 $m^2/g$, the pellets had a BET surface area of 1802 $m^2/g$.

Isotherm fitting was performed using Athena Visual Studio 14.0 (Athena Visual Software, Inc.).

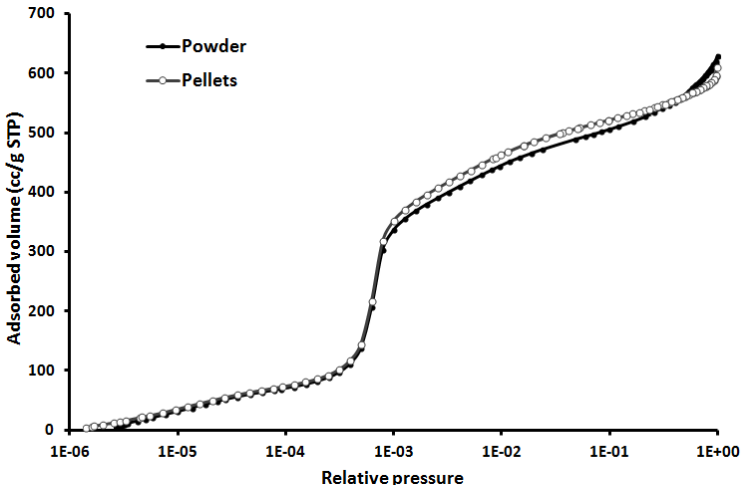


Figure S.1: Argon (87K) porosimetry on HKUST-1 powder (before pelletization) and pellets.

A 10 cm long stainless steel column with 2.54 mm internal diameter was packed with the pellets and regenerated by heating the column to 373K for 1 hour followed by further regenerating at 453K overnight, all under nitrogen flow. Breakthrough based adsorption capacities were calculated with the following formulae:

$$\mu_i = \int_0^{\infty} \left( 1 - \frac{C_i(t)}{C_{i,\,feed}} \right) dt$$

$$q_i = \frac{F.C_{i,\,feed}.(\mu_i - t_{dead})}{m_{ads}}$$

Here $C_i$ and $C_{i,feed}$ are the measured concentration (mol/m³) and feed concentration respectively. F is the volumetric flow rate (m³/s), $t_{dead}$ (s) is the dead time of the experimental set-up and $m_{ads}$ the mass of adsorbent.

Methanol (>99.9%, Sigma Aldrich) and *n*-hexane (>96%, Biosolve) loaded nitrogen (>99.998%, Air Liquide) streams were produced using temperature controlled saturators. These streams were fed to the regenerated column, and the column's outlet was monitored using a mass spectrometer at m/z ratios of 31 (methanol) and 43 (*n*-hexane). Further details regarding the experimental set-up can be found elsewhere (5).

The m/z-43 signal was corrected for the baseline drift of the mass spectrometer, as shown in figure S.2. The experimental breakthrough results are summarized in table S.1. Before this baseline correction, the total adsorbed amounts (on volume basis) for the equimolar breakthrough experiments were calculated at ca. 740 µl/g at high total vapor pressures. After baseline correction, this becomes ca. 670 µl/g (table S.1), more in line with the pure

component uptakes measured at similar high vapor pressures; ca. 680 µl/g for *n*-hexane and ca. 650 µl/g for methanol.

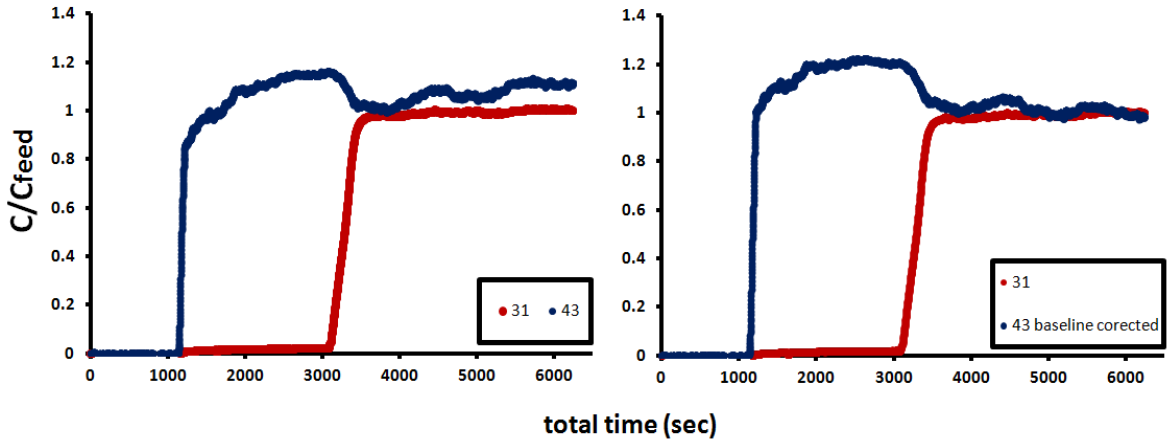


Figure S.2: Mass spectrometer output for the breakthrough of an equimolar methanol/*n*-hexane mixture on HKUST-1 (313K) at 11 kPa total vapor pressure before (Left) and after (Right) baseline correction of the 43 (*n*-hexane) m/z signal.

**Table S.1: Experimental results for binary breakthrough experiments with equimolar methanol/*n*-hexane mixtures on HKUST-1 at 313K.**

| *Total vapor pressure (Pa)* | *Selectivity methanol/ n-hexane* | *Methanol adsorbed (mol/kg)* | *n-hexane adsorbed (mol/kg)* | *Total adsorbed (mol/kg)* | $y_{MeOH}$ | *Total adsorbed (µl/g) ** |
|---|---|---|---|---|---|---|
| 11 300 | 4.12 | 9.0 | 2.2 | 11.2 | 0.50 | 667 |
| 7 250 | 3.60 | 8.6 | 2.4 | 11.0 | 0.50 | 677 |
| 4 250 | 3.12 | 7.9 | 2.6 | 11.6 | 0.49 | 683 |
| 2 700 | 3.85 | 7.6 | 2.0 | 9.6 | 0.49 | 586 |

* Calculated using the liquid densities of *n*-hexane and methanol at 313K.

For comparison, the IAST procedure was also applied for an apolar MOF, ZIF-8. The methanol isotherm data (323K) are taken from Cousin Saint Remi et al. (6) The *n*-hexane gravimetrical isotherm was obtained on a commercial Basolite Z1200 (ZIF-8) sample in a similar manner as for HKUST-1. The experimental temperature was 323K, while activation was performed at 453K for 4 hours.

## 2. Adsorption of argon compared to *n*-hexane and methanol adsorption

Argon porosimetry measurements were performed on a Quantasorb Autosorb AS-1 (Quantachrome Instruments, USA) device at 87K. Figure S.3 shows the argon porosimetry (87K) combined with the *n*-hexane and methanol isotherms obtained by gravimetric (313K) measurements (static method) converted to volume basis using the liquid density. The saturation capacity of the S1 cages is estimated to be near 15 % of the total pore volume, as shown in table S.2. The red line indicates this estimated saturation capacity of the S1 cages (based on 15% of the measured argon uptake at a relative pressure of 0.95), the preferential adsorption sites for argon at low pressure as shown in a previous study by Krungleviciute et al (7). This capacity agrees reasonably well with the onset of the second adsorption step for argon. The *n*-hexane allocating procedure (see below) utilizes a Langmuir equation with a saturation capacity of 1 *n*-hexane molecule per S1 cage. The Langmuir plot is given by the blue line in figure S.3, where the saturation plateau corresponds well with saturation of the estimated pore volume of the S1 cages.

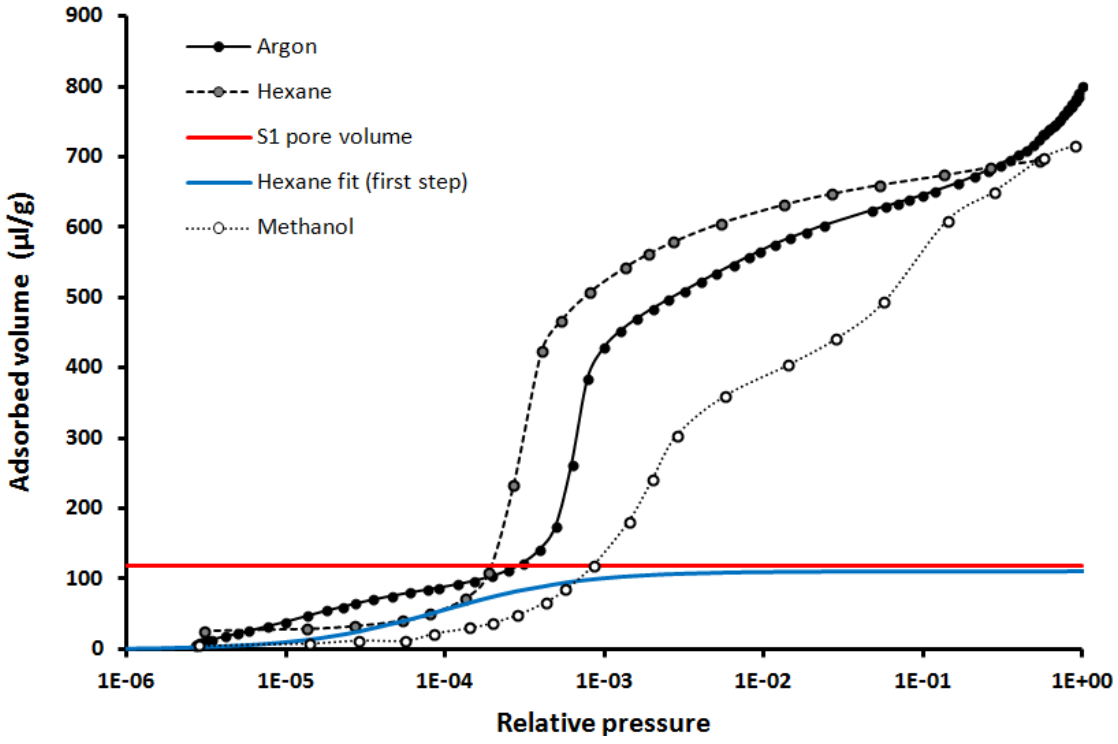


Figure S.3: Argon (87K) and *n*-hexane and methanol (313K) adsorption isotherms expressed as adsorbed volume (µl/g). The red line indicates the estimated S1 saturation capacity, the blue line the Langmuir fit applied to the first *n*-hexane step.

**Table S.2: Estimation of contributions of S1, L2 and L3 cages for argon.**

| Cage type | Estimated cage diameter (Å) | N° per HKUST-1 unit cell | Pore volume per HKUST-1 unit cell (Å³) | % |
|---|---|---|---|---|
| **S1** | 5 | 8 | 524 | **14.6** |
| **L2** | 9 | 4 | 1527 | **42.7** |
| **L3** | 9 | 4 | 1527 | **42.7** |

The pore size distribution of HKUST-1 powder based on the argon isotherm is shown in figure S.4 and reveals a bimodal distribution, i.e. the smaller S1 cages and the combined larger L2 and L3 cages.

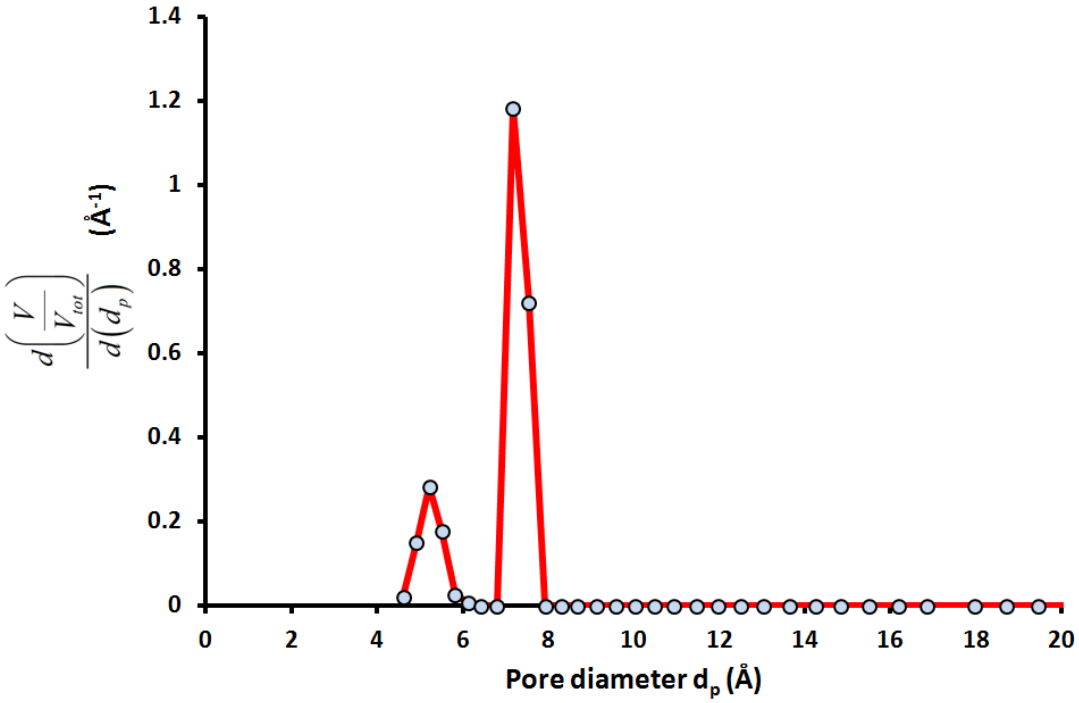


Figure S.4: Pore size distribution of HKUST-1 powder obtained from argon (87K) porosimetry and using the Quantachrome ASiQwin software (model: Ar (87K) on carbon, cylindrical pores, NLDFT adsorption branch).

## 3. Isotherm allocation

The experimental methanol and *n*-hexane isotherms are fragmented and parts are attributed to the S1, L2 and L3 cages identified in the HKUST-1 structure. We have identified only 3 adsorption locations in the structure. A more detailed adsorption mechanism including other adsorption sites, for example near the pore openings (windows) (8,9) is not considered.

**METHANOL**

The experimental two-step adsorption isotherm of methanol (313K) was fitted using a double Sips model:

$$q_{MeOH} = \frac{q_{MeOH,SAT1}.K_{MeOH,1}.p_{MeOH}^{\ n1}}{1+K_{MeoH,1}.p_{MeOH}^{\ n1}} + \frac{q_{MeOH,SAT2}.K_{MeOH,2}.p_{MeOH}^{\ n2}}{1+K_{MeoH,2}.p_{MeOH}^{\ n2}}$$

For methanol, the first Sips part describes the initial (low vapor pressure) adsorption step. The initial step (here given by the second Sips part above) has been assigned to filling of the L3 cages (1). Also, some of the first methanol molecules to adsorb have also been found in or near the S1 pockets (1,8). For this model, we have assumed the initial step in the methanol isotherm to occur solely due to filling of the L3 cages.

$$q_{MeOH,L3,SAT} = q_{MeOH,SAT2}$$
$$K_{MeOH,L3} = K_{MeOH,2}$$
$$\kappa = n2$$

The isotherm expression for the L3 cages thus becomes:

$$q_{MeOH,L3} = \frac{q_{MeOH,L3,SAT}.K_{MeOH,L3}.p_{MeOH}^{\ \kappa}}{1+K_{MeoH,L3}.p_{MeOH}^{\ \kappa}}$$

The Sips part describing the second adsorption step in the original fit is allocated to the combined behavior of the L2 and S1 cages. Based on the cages estimated internal diameter, occurrence and spherical cages, 75% of the Sips model capacity is allocated to the larger L2 cages and 25% to the smaller S1 cage (Table S.3).

$$q_{MeOH,S1,SAT} = 0.25 q_{MeOH,SAT1} \qquad q_{MeOH,L2,SAT} = 0.75 q_{MeOH,SAT1}$$
$$K_{MeOH,S1} = K_{MeOH,1} \qquad K_{MeOH,L2} = K_{MeOH,1}$$
$$\varepsilon = n1 \qquad \gamma = n1$$

Accordingly, 2 Sips isotherms (for the L2 cages and S1 cages) result from a single Sips isotherm:

$$q_{MeOH,S1} = \frac{q_{MeOH,S1,SAT} \cdot K_{MeOH,S1} \cdot p_{MeOH}{}^{\varepsilon}}{1 + K_{MeoH,S1} \cdot p_{MeOH}{}^{\varepsilon}}$$

$$q_{MeOH,L2} = \frac{q_{MeOH,L2,SAT} \cdot K_{MeOH,L2} \cdot p_{MeOH}{}^{\gamma}}{1 + K_{MeoH,L2} \cdot p_{MeOH}{}^{\gamma}}$$

**Table S.3: Estimation of contributions of L3 and S1 cages for methanol.**

| Cage type | Estimated cage diameter (Å) | N° per HKUST-1 unit cell | Pore volume per HKUST-1 unit cell (Å³) | % |
|---|---|---|---|---|
| **L3** | 9 | 4 | 1527 | **74.5** |
| **S1** | 5 | 8 | 524 | **25.5** |

The full methanol isotherm is now represented by:

$$q_{MeOH} = \frac{q_{MeOH,S1,SAT} \cdot K_{MeOH,S1} \cdot p_{MeOH}{}^{\varepsilon}}{1 + K_{MeoH,S1} \cdot p_{MeOH}{}^{\varepsilon}} + \frac{q_{MeOH,L2,SAT} \cdot K_{MeOH,L2} \cdot p_{MeOH}{}^{\gamma}}{1 + K_{MeoH,L2} \cdot p_{MeOH}{}^{\gamma}} + \frac{q_{MeOH,L3,SAT} \cdot K_{MeOH,L3} \cdot p_{MeOH}{}^{\kappa}}{1 + K_{MeoH,L3} \cdot p_{MeOH}{}^{\kappa}}$$

The color code red/blue/green corresponds to the cages S1/L2/L3 respectively, as indicated in Figure 1.

**N-HEXANE**

For *n*-hexane, the experimental isotherm (313K) was fitted using a Langmuir and double Sips model.

$$q_{Hex} = \frac{q_{Hex,SAT1} \cdot K_{Hex,1} \cdot p_{Hex}}{1 + K_{Hex,1} \cdot p_{Hex}} + \left( \frac{q_{Hex,SAT2} \cdot K_{Hex,2} \cdot p_{Hex}{}^{m2}}{1 + K_{Hex,2} \cdot p_{Hex}{}^{m2}} + \frac{q_{Hex,SAT3} \cdot K_{Hex,3} \cdot p_{Hex}{}^{m3}}{1 + K_{Hex,3} \cdot p_{Hex}{}^{m3}} \right)$$

First, the Langmuir model was fitted to the initial step of the isotherm, assuming a saturation capacity of 8 molecules per HKUST-1 unit cell.

$$q_{Hex,SAT1} = 8 \frac{molecules}{HKUST1 - unitcell}$$

In the next step, the double Sips model, combined with the already determined Langmuir fit, was fitted on the full isotherm.

Allocation of the fitted model above proceeds as follows:

The Langmuir isotherm is attributed to the S1 cages.

$$q_{Hex,S1,SAT} = q_{Hex,SAT1}$$
$$K_{Hex,S1} = K_{Hex,1}$$

$$q_{Hex,S1} = \frac{q_{Hex,S1,SAT}.K_{Hex,S1}.p_{Hex}}{1+K_{Hex,S1}.p_{Hex}}$$

The double Sips part of the original fit is allocated to the combined *n*-hexane adsorption in the L2 and L3 cages. This Sips part is divided in 2 equal parts, corresponding to the L2 cages and the L3 cages (Table S.4). This is achieved by adjusting the saturation values.

$$q_{Hex,L2,SATa} = q_{Hex,L3,SATa} = 0.5q_{Hex,SAT2} \qquad q_{Hex,L2,SATb} = q_{Hex,L3,SATb} = 0.5q_{Hex,SAT3}$$
$$K_{Hex,L2,a} = K_{Hex,L3,a} = K_{Hex,2} \qquad K_{Hex,L2,b} = K_{Hex,L3,b} = K_{Hex,3}$$
$$\alpha = m2 \qquad \beta = m3$$

Thus we obtain new double Sips expressions to qualitatively describe the adsorption in the L2 and L3 cages.

$$q_{Hex,L2} = \left( \frac{q_{Hex,L2,SATa}.K_{Hex,L2,a}.p_{Hex}{}^{\alpha}}{1+K_{Hex,L2,a}.p_{Hex}{}^{\alpha}} + \frac{q_{Hex,L2,SATb}.K_{Hex,L2,b}.p_{Hex}{}^{\beta}}{1+K_{Hex,L2,b}.p_{Hex}{}^{\beta}} \right)$$
$$q_{Hex,L3} = \left( \frac{q_{Hex,L3,SATa}.K_{Hex,L3,a}.p_{Hex}{}^{\alpha}}{1+K_{Hex,L3,a}.p_{Hex}{}^{\alpha}} + \frac{q_{Hex,L3,SATb}.K_{Hex,L3,b}.p_{Hex}{}^{\beta}}{1+K_{Hex,L3,b}.p_{Hex}{}^{\beta}} \right)$$

**Table S.4: Estimation of contributions of L2 and L3 cages for *n*-hexane.**

| Cage type | Estimated cage diameter (Å) | N° per HKUST-1 unit cell | Pore volume per HKUST-1unit cell (Å³) | % |
|---|---|---|---|---|
| **L2** | 9 | 4 | 1527 | **50.0** |
| **L3** | 9 | 4 | 1527 | **50.0** |

The full *n*-hexane isotherm is now represented by combining the contributions of the S1, L2 and L3 cages, yielding the same results as the original (non-allocated) fitting:

$$q_{Hex} = \frac{q_{Hex,S1,SAT} \cdot K_{Hex,S1} \cdot p_{Hex}}{1 + K_{Hex,S1} \cdot p_{Hex}}$$

$$+ \left( \frac{q_{Hex,L2,SATa} \cdot K_{Hex,L2,a} \cdot p_{Hex}^{\alpha}}{1 + K_{Hex,L2,a} \cdot p_{Hex}^{\alpha}} + \frac{q_{Hex,L2,SATb} \cdot K_{Hex,L2,b} \cdot p_{Hex}^{\beta}}{1 + K_{Hex,L2,b} \cdot p_{Hex}^{\beta}} \right)$$

$$+ \left( \frac{q_{Hex,L3,SATa} \cdot K_{Hex,L3,a} \cdot p_{Hex}^{\alpha}}{1 + K_{Hex,L3,a} \cdot p_{Hex}^{\alpha}} + \frac{q_{Hex,L3,SATb} \cdot K_{Hex,L3,b} \cdot p_{Hex}^{\beta}}{1 + K_{Hex,L3,b} \cdot p_{Hex}^{\beta}} \right)$$

The color code red/blue/green corresponds to the cages S1/L2/L3 respectively, as indicated in Figure 1.

## 4. IAST on apolar MOF ZIF-8

For comparison to HKUST-1, IAST was applied to the adsorption of the same methanol/*n*-hexane mixture on the apolar MOF zinc-2-methyl-imidazole (ZIF-8), which does not contain free metal sites. Figure S.5 shows that both adsorbates have a similar pore filling when the gravimetric data are converted using the liquid density at 323K. Figure S.5 also shows the isotherm fits used for the IAST method. Figure S.6 shows the *n*-hexane over methanol selectivity to drop continuously with increasing total vapor pressure (increasing methanol over *n*-hexane selectivity), rather than maintain quasi constant as was predicted for HKUST-1. This predicted behavior is qualitatively similar to the L2 and S1 cages of HKUST-1.

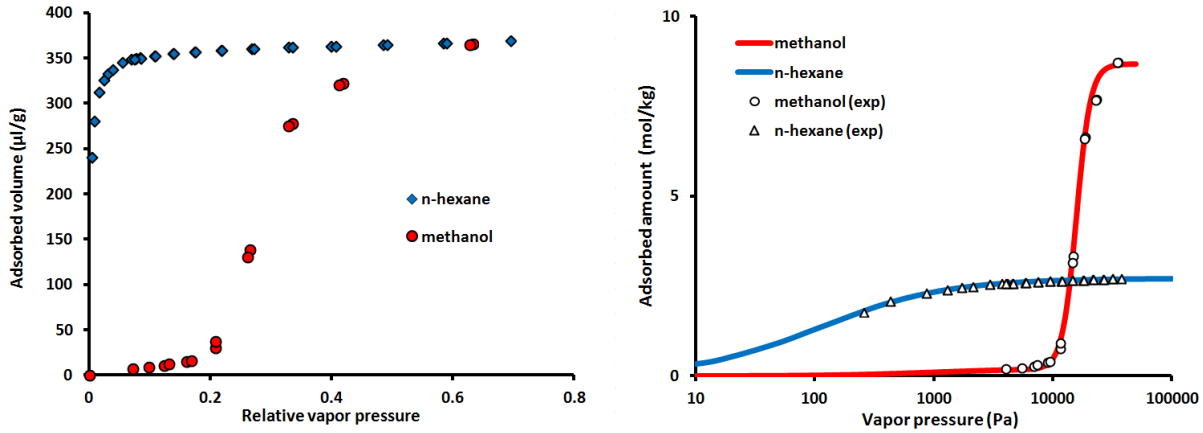


Figure S.5: Experimental *n*-hexane and methanol (323K) isotherm on ZIF-8. Left: Expressed as adsorbed volume per gram of adsorbent (calculated using the liquid densities at 323K). Right: The experimental data and isotherm fits of *n*-hexane and methanol (323K) on ZIF-8 at 323 K.

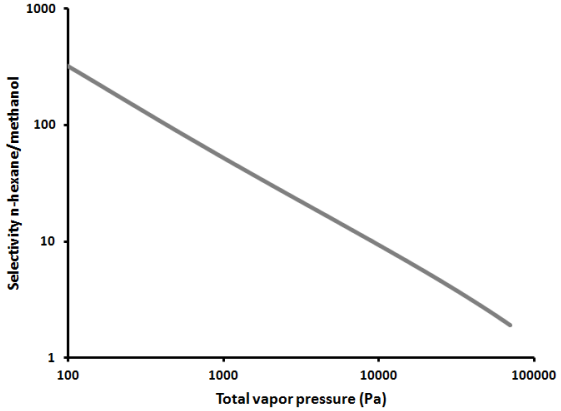


Figure S.6: Predicted selectivity of *n*-hexane over methanol for an equimolar binary mixture for ZIF-8 (323K) using IAST.

**References**

(1) Van Assche, T.R.C.; Duerinck, T.; Gutiérrez-Sevillano, J.J.; Calero, S.; Baron, G.V.; Denayer, J.F.M. High Adsorption Capacities and Two-Step Adsorption of Polar Adsorbates on Copper-Benzene-1,3,5-tricarboxylate Metal-Organic Framework. *J. Phys. Chem. C* **2013**, *117*, 18100-18111.

(2) Castillo, J.M.; Vlugt, T.J.H.; Calero, S. Understanding Water Adsorption in Cu-BTC Metal-Organic Frameworks. *J. Phys. Chem. C* **2008**, *112*, 15934-15939.

(3) Cychosz, K.A.; Matzger, A.J. Water Stability of Microporous Coordination Polymers and the Adsorption of Pharmaceuticals from Water. *Langmuir* **2010**, *26*, 17198-17202.

(4) Peterson, G.W.; DeCoste, J.B.; Glover, T.G.; Huang, Y.; Jasuja, H.; Walton, K.S. Effects of pelletization pressure on the physical and chemical properties of the metal-organic frameworks $Cu_3(BTC)_2$ and UiO-66. *Microporous Mesoporous Mater.* **2013**, *179*, 48-53.

(5) Van Assche T.R.C.; Denayer J.F.M. Fabrication and separation performance evaluation of a metal-organic framework based microseparator device. *Chem. Eng. Sci.* **2013**, *95*, 65-72.

(6) Cousin Saint Remi, J.; Rémy, T.; Van Hunskerken, V.; van de Perre, S.; Duerinck, T.; Maes, M.; De Vos, D.; Gobechiya, E.; Kirschhock, C.E.A.; Baron, G.V.; Denayer, J.F.M. Biobutanol Separation with the Metal-Organic Framework ZIF-8. *ChemSusChem* **2011**, *4*, 1074-1077.

(7) Krungleviciute, V.; Lask, K.; Heroux, L.; Migone, A.D.; Lee, J.Y.; Li, J.; Skoulidas, A. Argon Adsorption on $Cu_3$(Benzene-1,3,5-tricarboxylate)$_2(H_2O)_3$ Metal-Organic Framework. *Langmuir* **2007**, *23*, 3106-3109.

(8) Gutiérrez-Sevillano, J.J.; Vicent-Luna, J.M.; Dubbeldam, D.; Calero, S. Molecular Mechanisms for Adsorption in Cu-BTC Metal Organic Framework, *J. Phys. Chem. C* **2013**, *117*, 11357-11366.

(9) Calero, S.; Gutiérrez-Sevillano, J.J.; García-Pérez, E. Effect of the molecular interactions on the separation of nonpolar mixtures using Cu-BTC metal-organic framework. *Microporous Mesoporous Mater.* **2013**, *165*, 79-83.